Trans Indian Inst Met (2026) 79:33
https://doi.org/10.1007/s12666-026-03797-x

REVIEW ARTICLE

A Review on Sulphur Thermodynamics in Liquid Iron

Anže Bajželj[1,2] · Tilen Balaško[2] · Jaka Burja[1,2]

Received: 18 March 2025 / Accepted: 15 January 2026

Abstract Sulphur in steel, primarily introduced during ironmaking through coke, forms sulphide non-metallic inclusions, which adversely affect hot working processes and steel properties, reducing impact toughness, ductility, weldability, and corrosion resistance. To mitigate these effects, desulphurisation techniques remove sulphur by forming stable sulphides in the slag phase, primarily through ladle slag treatment. Understanding sulphur thermodynamics in liquid iron is essential for controlling its solubility and activity during steelmaking. This study reviews existing methods for determining sulphur solubility in iron melts, highlighting challenges due to its high solubility and complex phase interactions. It also examines element-sulphur reactions and the conditions for sulphide formation. Overall, this work provides a comprehensive analysis of sulphur's role in steel metallurgy and offers insights to optimise desulphurisation practices for improved steel quality.

Keywords Steelmaking · Thermodynamics · Sulphur · Sulphides · Desulphurisation · Non-metallic inclusions

1 Introduction

Sulphur is a tramp element that is always found in steel in small amounts. Even at low concentrations, sulphur can decrease steel's impact toughness and ductility, negatively affect weldability, and reduce corrosion resistance in stainless steel. Its content is usually restricted by the upper limit of 0.03 or 0.035 wt% S. Steels with extremely low sulphur contain less than 0.001 wt% S. In the case of elevated sulphur content in the steel melt, FeS can form, which remains in a liquid state at hot working temperatures. This causes hot shortness, making hot forming of the steel impossible [1–4].

Sulphur is introduced into the ironmaking and steelmaking processes through coke, ferroalloys, and ore [5–11]. Coke serves both as a reduction agent and as a fuel in the blast furnace. Coke's sulphur concentrations vary according to coal quality. During pig iron production, up to 5 wt% carbon and up to 0.05 wt% sulphur is dissolved in hot metal [12, 13].

Figure 1 presents Fe-S phase diagram, calculated by the ThermoCalc program (Thermo-Calc 2017a, Thermo-Calc Software AB, Stockholm, Sweden) using the TCFE8.1 database. In the literature, a variety of records describing the iron-sulphur phase diagram and providing equilibrium values of the element's solubility in the iron melt can be found [14–19]. The authors present the thermodynamic models used to determine equilibrium states in the phase diagram, including the solubility of sulphur in the iron melt. The solubility of sulphur in iron melt is high and depends on the reaction conditions between the melt, atmosphere, and slag. At concentrations above 35 wt% S, the melt is saturated with sulphur, and a gaseous phase (S_2) is formed. Sulphur solubility in the solid phase significantly decreases; the highest solubility of sulphur in the solid solution is 0.10 wt% at 1366 °C. At 988 °C and 31 wt% of sulphur, a eutectic reaction occurs, forming a solid solution of γ-Fe and the compound FeS from the melt [1, 2, 14–16, 20, 21]. The low melting temperature of the FeS-γ-Fe eutectic reaction is the cause of hot shortness in iron alloys. FeS forms at concentrations of dissolved sulphur in

✉ Anže Bajželj
anze.bajzelj@imt.si

[1] Institute of Metals and Technology, 1000 Ljubljana, Slovenia

[2] Department of Materials and Metallurgy, Faculty of Natural Sciences and Engineering, University of Ljubljana, 1000 Ljubljana, Slovenia

Published online: 28 January 2026

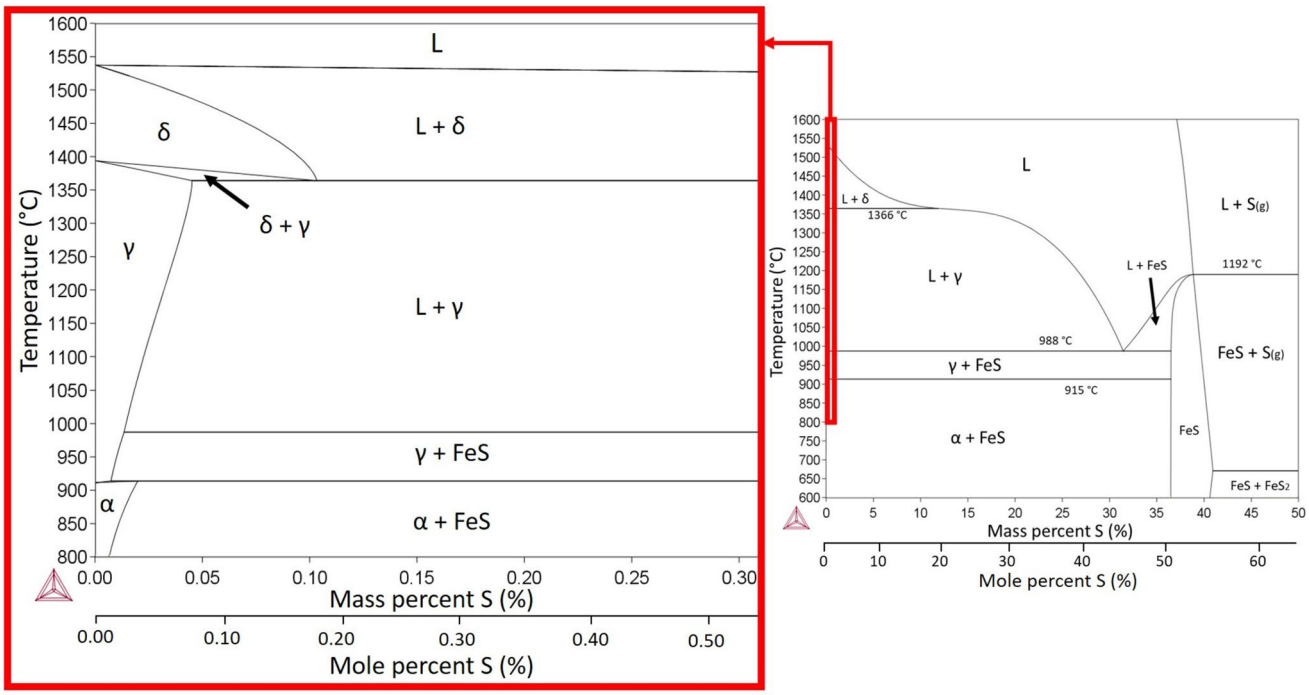

Fig. 1 Phase diagram of iron and sulphur

the solid solution higher than 100 ppm. Therefore, a liquid phase is present during hot deformation, weakening the grain boundaries and causing hot cracking.

To maintain the workability of the steel, the formation of FeS must be avoided by decreasing the sulphur solubility and activity in the steel. The formation of FeS can be mitigated by reducing the sulphur concentration in the melt to below 100 ppm. The second approach is to decrease the activity of the sulphur in the melt by introducing alloying elements such as Mn, Ca, Mg, Cr, Ti, etc., or to promote the formation of sulphides with these elements, which are more stable and remain in a solid state at hot working temperatures. Accurately predicting the formation of sulphides in steel requires precise knowledge of the concentration and activity of sulphur in the melt. However, due to the complex nature of the multiphase system involved, determining the exact sulphur content is exceptionally challenging. Therefore, in practice, a variety of empirical methods are used to determine the solubility of sulphur in the melt and in the slag [1, 2, 9, 11, 14, 16, 20, 22–26].

The present work attempts to present the challenges of determining the sulphur concentrations and activities in steel melt. Understanding the solubility and activity of sulphur is crucial for controlling its concentration and mechanism for sulphides formation. A literature review on the determination of sulphur solubility in iron and steel alloys is presented, along with typical representatives of sulphides. Based on literature data, some calculations for sulphide formation have been developed.

2 Solubility of sulphur in liquid iron

The phase diagram in Fig. 1 shows, that the solubility of sulphur in liquid iron is high. The melt's saturation with sulphur is achieved at a ratio of iron-to-sulphur mole fractions of 1:1; beyond the saturation limit, the gaseous phase is precipitated from the melt. By reducing the pressure above the steel melt, the solubility of gases in the melt decreases. This means that the equilibrium sulphur solubility could be potentially determined based on the partial pressure above the surface of the steel melt. The equilibrium solubility of sulphur in the melt can be determined using the expression for the solubility of ideal gases in solutions using Sievert's law.

Based on thermodynamic calculations, it is evident that elemental sulphur is stable in the gaseous state S_2 within the temperature range of iron and steel production [27, 28]. Sievert's law determines the solubility of gaseous elements in the melt, stating that the solubility of a gaseous element is proportional to the element's empirical constant and the square root of the partial pressure of the gas above the melt surface [1]. Equation (1) provides the dissolution of sulphur (S_2) in the iron melt; several formulations for calculating the Gibbs free energy of sulphur dissolution in diluted iron solution for the 1 wt% standard state has been reported in the

Table 1 Overview of $\Delta G^{\circ}_{(1)}$ and $\log(K_1)$ for sulphur an infinite dilution in liquid iron melt

	$\Delta G^{\circ}_{(1)}$ [J/mol]	$\log(K_{(1)})$
Sigworth et al. [29]	$-135{,}060+23.43\cdot T$	$7055/T-1.224$
Kato et al. [30]	$-125{,}104+18.45\cdot T$	$6535/T-0.964$
Sherman et al. [26]	$-131{,}880+22.05\cdot T$	$6889/T-1.152$

Table 2 Equilibrium pressure of dissolved sulphur at different temperatures and activities

	Temperature (K)			
	1823	1873	1923	1973
Activity	S_2 pressure (Pa)			
1.0	0.517	0.832	1.306	2.004
0.9	0.419	0.674	1.058	1.623
0.8	0.331	0.532	0.836	1.283
0.7	0.253	0.408	0.640	0.982
0.6	0.186	0.299	0.470	0.721
0.5	0.129	0.208	0.327	0.501
0.4	0.083	0.133	0.209	0.321
0.3	0.047	0.075	0.118	0.180
0.2	0.021	0.033	0.052	0.080
0.1	0.005	0.008	0.013	0.020

literature, with calculated values not deviating significantly [1, 2, 11, 16, 26, 29–31]. Table 1 summarizes the Gibbs free energies for the sulphur dissolution reaction in liquid iron. The Gibbs free energies of the dissolution reaction are highly negative, meaning that sulphur is well dissolved in the liquid iron.

$$\frac{1}{2}S_{2(g)} = [S] \tag{1}$$

$$K_S = \frac{a_S}{\sqrt{p_{S_2}}} = \frac{[wt.\%S]\cdot f_S}{\sqrt{p_{S_2}}} \tag{2}$$

Analogous to the calculation of nitrogen solubility in the iron melt [25], the equilibrium pressures of S_2 required to achieve the activity or solubility of sulphur in the melt at different temperatures were calculated. The results, presented in Table 2, confirm the high solubility of sulphur in the iron melt, with solubility decreasing as the sulphur pressure above the melt surface decreases. The calculations show that extremely low gas pressures are needed for the melt to become saturated with sulphur, making the determination of sulphur solubility in the melt challenging due to the very low pressures of the gaseous phase. Moreover, it can be inferred that due to the low concentration of gaseous sulphur above the melt surface, desulphurisation in a vacuum is both time-consuming and inefficient. The results also indicate that as the system temperature increases, the solubility of sulphur in the melt decreases, suggesting that desulphurisation is more efficient at higher temperatures.

The calculated equilibrium S_2 pressures presented in Table 2 are subject to several sources of theoretical uncertainty that arise from the thermodynamic parameters used in the modelling. The most important contribution originates from the differences between the published Gibbs free energy correlations for sulphur dissolution in liquid iron, as shown in Table 1, since substituting individual ΔG° expressions into Eq. (2) yields slightly different equilibrium constants and consequently noticeable variation in the calculated S_2 pressures. Additional uncertainty is associated with the activity coefficient of sulphur, whose value depends on the selected thermodynamic description and interaction parameters, even small variations in f_S directly influence the calculated sulphur activity and therefore the corresponding equilibrium pressure. The calculations are also sensitive to temperature, as ΔG° exhibits a strong temperature dependence, meaning that minor deviations in the assumed melt temperature can influence the predicted pressure values. Moreover, the application of Sievert's law assumes ideal-gas behaviour of S_2, which introduces a conceptual simplification at high temperatures. Despite these uncertainties, all calculated pressures remain extremely low, consistently confirming that the equilibrium concentration of gaseous sulphur above the melt surface is negligible and that direct determination of sulphur solubility from gas-phase measurements is impractical.

It has been demonstrated that determining sulphur content via gas pressure above the melt surface is extremely challenging due to the high solubility of the element in iron melts. The concentration of S_2 above the melt surface is negligibly low; therefore, the activity or solubility of sulphur in the melt can be assessed using the ratio of partial pressures in a gas mixture of H_2 and H_2S. Several researchers have established the relationship between temperature, pressure ratio, and sulphur activity and solubility in the melt. Based on the partial pressure ratio of H_2S to H_2 and the concentration of equilibrium dissolved sulphur, the reaction constant (3) has been determined, which allows for the calculation of the activity coefficient when the concentration of dissolved sulphur is known [26, 32–35]. However, this gas mixture is not encountered in steel production, making the method impractical for industrial applications. It is primarily useful for laboratory research.

$$\begin{aligned} &H_{2(g)} + [S] = H_2S_{(g)} \\ &\Delta G^{\circ}_{(3)} = 41170 + 27.36 \cdot T \end{aligned} \tag{3}$$

In the literature, there are several examples where researchers develop sensors for directly measuring sulphur activity in steel melts [36–38]. Similar to those used for

measuring oxygen activity, these sensors are reaction cells submerged in the steel melt. By measuring electromotive force, the activity of oxygen or sulphur is determined. However, since oxygen is also present in the steel melt and is more reactive than sulphur, it interferes with sulphur measurements. Current sulphur activity sensors have a narrow operating range, are complex to manufacture, and are therefore impractical on a large scale for industrial use.

Fundamental research on the solubility of sulphur in iron melt has been conducted at higher concentrations than those encountered in steelmaking practice. Research has been based on describing the equilibrium phase system Fe–S. However, sulphur proportions in practice are significantly lower but still problematic for FeS formation. At low concentrations of sulphur in the iron melt, we can consider the 1 wt% standard state or Raoult's standard state, where the activities of sulphur are equal to the product of the activity coefficient and the weight percent or mole fraction of dissolved element. For calculation of activity at 1 wt% standard state, Eq. (4) can be used. In addition to iron and sulphur, other elements are present in the steel melt, affecting both the solubility of sulphur and the formation of FeS. Based on Wagner's formalism, the mutual influence of elements in solution can be determined [39, 40]. The influence of dissolved elements on sulphur can be expressed by Eqs. (4), and (5).

$$a_S = f_S \cdot [\text{wt. \% S}] \tag{4}$$

$$\log f_S = \sum e_S^i \cdot [\text{wt. \% } i] \tag{5}$$

Table 3 provides interaction coefficients of element influence on sulphur in diluted iron solution at 1600 °C, with values varying among different authors [2, 29, 30, 41–47]. The values of interaction coefficients vary slightly, which is a result of the method used to determine them. At low concentrations of dissolved sulphur in the melt, the differences in activity are small. The addition of an element with a negative interaction coefficient value reduces the activity of sulphur in the solution while raising the solubility limit of sulphur. Figure 2 shows calculated values of sulphur activity in the diluted iron solution at 1600 °C at different interaction coefficients.

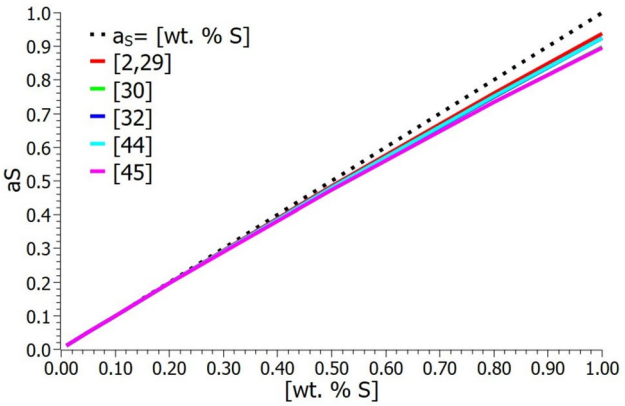

Fig. 2 Influence of sulphur content on the activity of sulphur in diluted iron solution at 1600 °C

It has been found that the solubility of sulphur in the liquid iron is high, which is confirmed by the low value of Gibbs free energy for the dissolution of the element. Consequently, directly determining the concentration of sulphur or its activity in the melt based on the pressure above the surface of the melt is difficult. To determine the activity of sulphur in the melt at low concentrations of the element, the 1 wt% standard state rule can be used.

3 Sulphides

It has been shown that exceeding a sulphur concentration of 100 ppm results in the formation of FeS, which negatively affects properties and significantly complicates the hot working of the steel, namely forging and rolling [1, 2, 9–11, 48–53]. Sulphur tends to form more stable sulphides, which can prevent the formation of FeS. Sulphides with manganese, calcium, and magnesium are commonly present in iron or steel production. These sulphides are more stable than FeS and remain solid at hot working temperatures, thus causing fewer production issues. Figure 3 shows the temperature dependence diagram of the Gibbs free energy

Table 3 Interaction coefficients e_S^i in diluted iron solution at 1600 °C

Al	C	Ca	Cr	Mg
0.035 [2, 29, 30]	0.11 [2, 29]	– 110 [2, 29] – 22.4 [45] – 106 [46]	– 0.011 [2, 29]	– 1.82 [47]
Mn	O	P	S	Si
– 0.026 [2, 29]	– 0.27 [2, 29]	0.29 [2, 29]	– 0.028 [2, 29, 46] – 0.046 [30] – 0.034 [32] – 0.0337 [43] – 0.047 [44]	0.063 [2, 29] 0.067 [43]

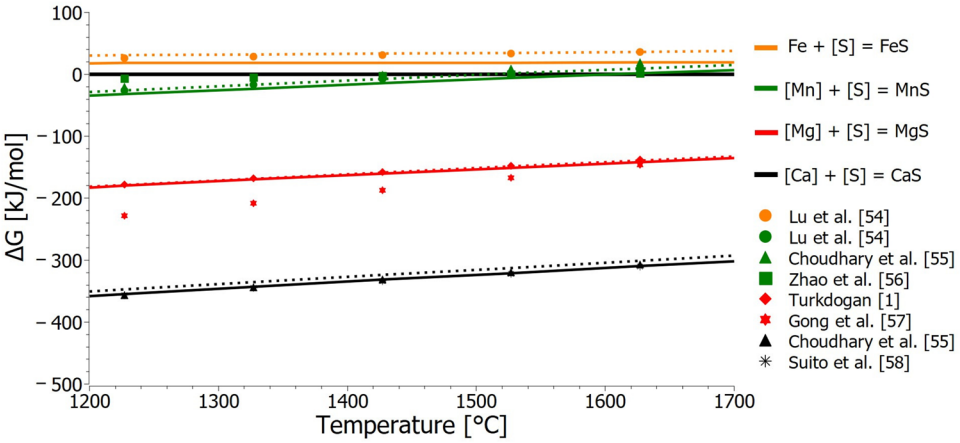

Fig. 3 Temperature dependence of Gibbs free energy for the formation of sulphides. Note: solid line, the thermodynamic data taken from HSC 8.0 database, Barin et al. [28], and Sigworth et al. [29], dotted line, the thermodynamic data taken from Barin et al. [28], and Sigworth et al. [29]. The diagram also marks points from other literature sources [1, 54–58]

Table 4 Gibbs free energies for reactions considered in calculating sulphides formation

Reaction	$\Delta G°$ [J/mol]	References
$1/2S_{(g)} = [S]$	$-135{,}060 + 23.43 \cdot T$	[29]
$Mn_{(s)} = Mn_{(l)}$	$12{,}058 - 7.949 \cdot T$	[28]
$Mn_{(l)} = [Mn]$	$4083.6 - 38.158 \cdot T$	[29]
$Mg_{(g)} = [Mg]$	$-78{,}690 + 70.8 \cdot T$	[1]
$Ca_{(l)} = Ca_{(g)}$	$153{,}640 - 87.544 \cdot T$	[28]
$Ca_{(g)} = [Ca]$	$-39{,}455 + 49.371 \cdot T$	[29]

for sulphide formation in the temperature range between 1200 and 1700 °C. The data for calculating the Gibbs free energies were taken from the software database HSC 8.0, as well as from other literature records of databases [1, 28, 29]. The enthalpies and entropies for chemical reactions (6) – (9) were obtained from HSC 8.0 software databases (solid lines in Fig. 3) and thermochemical data of pure substances [28] (dotted lines in Fig. 3). The energy change due to the dissolution of elements in iron melt at 1 wt% standard state was also incorporated, data are collected in Table 4 [1, 28, 29]. Calculated values are presented in Table 5, graphical representation is plotted in Fig. 3. Table 5 also contains data on Gibbs free energies for reactions from other literature sources. The calculated energies are included in the diagram in Fig. 3. In most cases, the data aligns with the calculated values presented in the present work [1, 54–58]. It is evident from the diagram, that the reaction between iron and sulphur is the least stable, meaning that the addition of calcium,

Table 5 Calculated Gibbs free energies for the formation of sulphides

Reaction	$\Delta G°$ [J/mol]	References	On Fig. 2
$Fe + [S] = FeS$	$-6876 + 23.43 \cdot T$	[1, 28, 29]	
	$-2642 + 12.22 \cdot T$	HSC 8.0 and [1, 28, 29]	
	$-9940 + 24.10 \cdot T$	[54]	
$[Mn] + [S] = MnS$	$-160{,}863 + 89.75 \cdot T$	[1, 28, 29]	
	$-161{,}122 + 85.90 \cdot T$	HSC 8.0 and [1, 28, 29]	
	$-165{,}415 + 92.93 \cdot T$	[54]	
	$-168{,}822 + 98.87 \cdot T$	[55]	
	$-39{,}469 + 21.71 \cdot T$	[56]	
$[Mg] + [S] = MgS$	$-329{,}001 + 99.92 \cdot T$	[1, 28, 29]	
	$-326{,}440 + 97.39 \cdot T$	HSC 8.0 and [1, 28, 29]	
	$-325{,}941 + 98.80 \cdot T$	[1]	
	$-537{,}259 + 205.75 \cdot T$	[57]	
$[Ca] + [S] = CaS$	$-522{,}239 + 116.65 \cdot T$	[1, 28, 29]	
	$-530{,}285 + 116.67 \cdot T$	HSC 8.0 and [1, 28, 29]	
	$-542{,}531 + 124.15 \cdot T$	[55]	
	$-530{,}900 + 116.2 \cdot T$	[58]	

magnesium, or manganese, makes the formation of FeS limited. Calcium forms the most stable sulphide, followed by sulphides with magnesium and manganese. The solubility of calcium and magnesium sulphides is low, and the formation of non-metallic inclusions occurs already in the melt, enabling sulphur removal during the production process of iron alloys [1, 59–62]. The solubility of manganese sulphides is somewhat higher, so particles form mainly during solidification, often as a result of segregations between dendritic grains.

$$Fe + [S] = FeS \tag{6}$$

$$Mn + [S] = MnS \tag{7}$$

$$Mg + [S] = MgS \tag{8}$$

$$Ca + [S] = CaS \tag{9}$$

The Gibbs free energies listed in Table 5 show noticeable variation, especially for MnS and MgS, primarily because the cited authors use different thermodynamic databases, reference states, and methods for deriving ΔG°. Some datasets rely on pure-substance thermochemical tables, others on assessed databases such as HSC, while certain values are obtained by extrapolating limited high-temperature measurements. In addition, not all sources apply the same standard state for dissolved elements in liquid iron, which leads to systematic shifts in the linear ΔG° expressions and largely explains the deviations observed in references [56] and [57]. Despite these numerical differences, all data consistently show the same stability order of sulphides, CaS being the most stable, followed by MgS and MnS, while FeS is the least stable.

3.1 Calcium sulphides

Calcium solubility in liquid steel or hot metal is low, Fig. 4 shows the solubility of calcium as a function of the partial pressure of $Ca_{(g)}$ in the iron melt at various temperatures. As the temperature increases, the solubility of calcium decreases, which can be attributed to the high vapour pressure of the element [1, 29, 63]. The formation of CaS directly from dissolved Ca and S is practically impossible, therefore the desulphurisation efficiency with calcium is poor. Desulphurisation is far more appropriate in the case of lime addition, as the oxide is more stable and remains in the melt for a longer time.

Figure 5 shows the calculated equilibrium solubility of calcium and sulphur in the melt at various temperatures. As the temperatures of the system increase, the solubility limit of the elements decreases, indicating a higher possibility

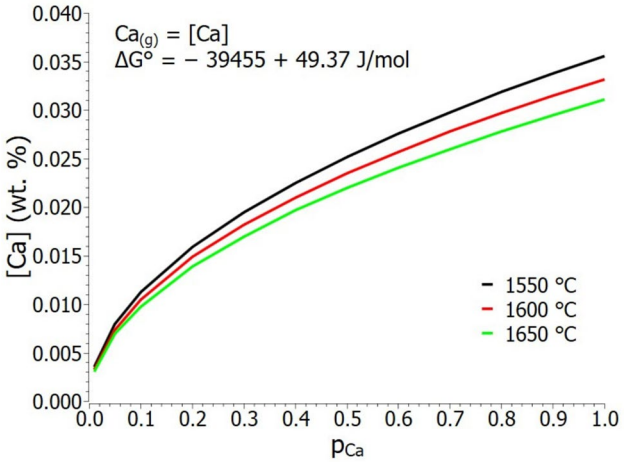

Fig. 4 Equilibrium solubility of calcium as a function of partial pressure at various temperatures in liquid iron [29]

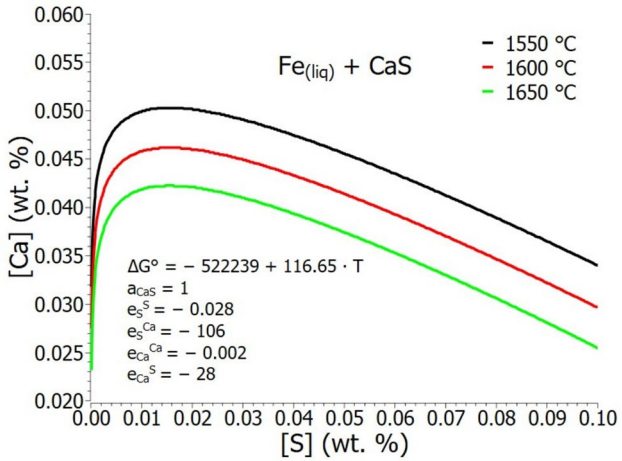

Fig. 5 Equilibrium solubility of Ca and S in liquid iron at different temperatures [1, 2, 28, 29, 46]

of CaS formation at elevated temperatures. The calculated values reveal that the solubility limit for CaS formation is exceptionally high, making it unrealistic to achieve such calcium saturation under practical conditions. Consequently, desulphurisation using calcium proves to be ineffective due to calcium's high boiling point and vapour pressure. When calcium is injected, vapours form within the melt, leading to localized saturation and subsequent reactions with sulphur.

Desulphurisation with calcium involves the use of lime, during which the oxide decomposes and CaS is formed, as described in Eq. (10). Thermodynamic data has been used to determine the Gibbs free energy for this reaction [1, 28, 29]. The desulphurisation process occurs on CaO particles, where the formation of CaS creates a barrier that impedes the diffusion of CaO, thereby influencing the kinetics of

desulphurisation [9, 51, 52]. During the reaction, CO is released, which aids in mixing the melt and increasing the rates of chemical reactions. As shown, carbon also participates in the reaction, and higher carbon activity in the melt results in more intense desulphurisation. At higher carbon activities, the oxygen activity in the melt is reduced, which further enhances the desulphurisation process.

$$CaO + [S] + [C] = CaS + CO_{(g)}$$
$$\Delta G^{\circ}_{(10)} = 88187 - 71.603 \cdot T \quad (10)$$

As stated by Magnelov et al. [51], in the case of elevated silicon content in the melt, the desulphurisation reaction can be expressed by the following Eq. (11). Based on the thermodynamic data, the Gibbs free energy for the given reaction was determined [1, 28, 29].

$$4CaO + 2[S] + [Si] = 2CaS + 2CaO \cdot SiO_2$$
$$\Delta G^{\circ}_{(11)} = -445341 + 119.586 \cdot T \quad (11)$$

Desulphurisation of hot metal can also be carried out with calcium carbide, producing CaS and carbon as products. Magnelov et al. [51, 52] mentioned that calcium carbide typically contains up to 30 wt% CaO, which significantly affects the desulphurisation process.

$$CaC_2 + [S] = CaS + 2C \quad (12)$$

CaS can also form during the modification of alumina non-metallic inclusions. In the ladle treatment of aluminium-killed steels, calcium is added to modify these hard alumina non-metallic inclusions. With the appropriate amount of calcium added, liquid calcium aluminate non-metallic inclusions are formed, which improves the castability of the steel, reduces issues with the clogging of submerged entry nozzles, and enhances the steel's mechanical properties. Sulphur dissolved in the steel melt binds to the modified calcium aluminates. If an excessive amount of calcium is added, the sulphide capacity of the inclusions increases, allowing for the binding of more sulphur. Choudhary and Ghosh [55] noted that as the steel cools, the solubility of sulphur in the non-metallic inclusions decreases, leading to the formation of CaS. An excess of calcium in the melt results in the formation of solid CaS, which hinders casting and negatively affects the mechanical properties of the steel [42, 55, 64].

3.2 Magnesium Sulphides

The solubility of magnesium in iron melt is low, which can mainly be attributed to the high vapour pressure and low boiling point of this element. Data on the solubility of magnesium in iron melt vary significantly, which can be attributed to the high reactivity of Mg. When considering the dissolution energy of magnesium in diluted liquid iron, the literature reveals deviations due to the reactivity of the element, leading to challenges in measurement execution [1, 9, 49, 53, 62]. Table 6 presents the Gibbs free energies from different literature sources. Figure 6 shows the solubility diagram of magnesium in iron melt as a function of partial pressure at different temperatures. According to data from Turkdogan [1], the solubility of magnesium decreases with increasing temperature. However, other literature sources show the opposite trend [53, 57, 60]. Based on the literature, it is evident that the data dispersion is quite large, making it difficult to determine the equilibrium solubility. In all cases, however, it can be confirmed that the solubility of the element is strongly dependent on the partial pressure of magnesium vapours.

Table 6 Gibbs free energies for the dissolution of magnesium vapours in iron melt [1, 53, 57]

Reaction	ΔG° [J/mol]	References
$Mg_{(g)} = [Mg]$	$-78{,}690 + 70.8 \cdot T$	[1]
	$117{,}400 - 31.4 \cdot T$	[57]
	$-331{,}459 + 172.09 \cdot T$	[53]

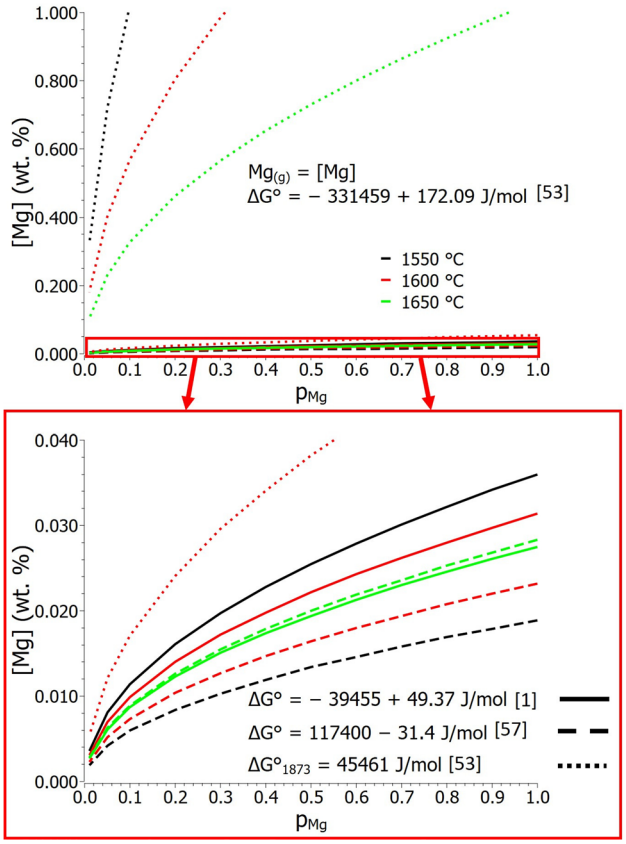

Fig. 6 Solubility of Mg in liquid iron at different temperatures. Data of Gibbs free energies from [1, 53, 57]

Magnesium sulphides are encountered in the desulphurisation of hot metal, in other applications, working with magnesium is not practical due to the high vapour pressure. A large amount of sulphur is dissolved in the hot metal, which mainly originates from coke. Due to the high carbon content, the activity of sulphur is high and therefore the desulphurisation of the hot metal before further processing is extremely reasonable. Several techniques are employed for hot metal desulphurisation, generally involving the addition of magnesium, lime, or calcium carbide, in the majority of industrial cases, a combination of reagents is utilized [2, 9, 10, 23, 49, 52, 65, 66]. To remove 1 kg of sulphur theoretically, 0.75 kg of magnesium is needed; in the case of desulphurisation with calcium or lime, the quantity increases to 1.25 kg of added pure calcium.

The processing temperatures for hot metal desulphurisation range between 1150 and 1400 °C, significantly lower than those for steel melt processing. Magnesium has a low boiling point, making it suitable for desulphurisation at hot metal processing temperatures. Yang et al. [61] mentioned the technique of hot metal desulphurisation using magnesium vapours generated by the carbothermic decomposition of magnesium oxide. Irons and Guthrie [66] described the kinetics of desulphurisation and found that desulphurisation is more intense with magnesium dissolved in the melt than with magnesium bubbles. The major challenge with magnesium is its low boiling point and high vapour pressure, leading to the low solubility of magnesium in iron alloys. After adding magnesium, which is usually injected into the hot metal, some of the magnesium evaporates, binding and removing sulphur with magnesium bubbles, while some magnesium dissolves in the melt, followed by desulphurisation according to the lower reactions [9, 10, 65]:

$$Mg_{(g)} + [S] = MgS \tag{13}$$

$$[Mg] + [S] = MgS \tag{14}$$

The solubility of magnesium increases proportionally with the increasing partial pressure of magnesium above the surface. Trojan and Flinn [60] presented that magnesium solubility increases with the carbon concentration in the solution and increasing temperature. With the system temperature rising, the partial pressure of magnesium increases, and the element's solubility is higher; however, due to more intensive evaporation, magnesium loss from the melt is substantially higher [52, 60, 61]. For hot metal desulphurisation with magnesium, a smaller amount of the element is needed, but the stability of MgS is lower compared to CaS. The stability of MgS is low, and it can react with oxygen from the atmosphere above the melt surface. To prevent re-sulfurization of the hot metal, lime is added in addition to magnesium, where lime reacts with MgS, and

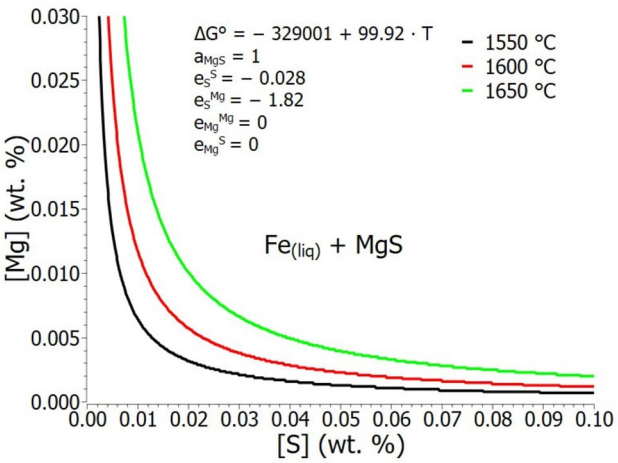

Fig. 7 Equilibrium solubility of Mg and S in liquid iron at different temperatures [1, 2, 28, 29, 53]

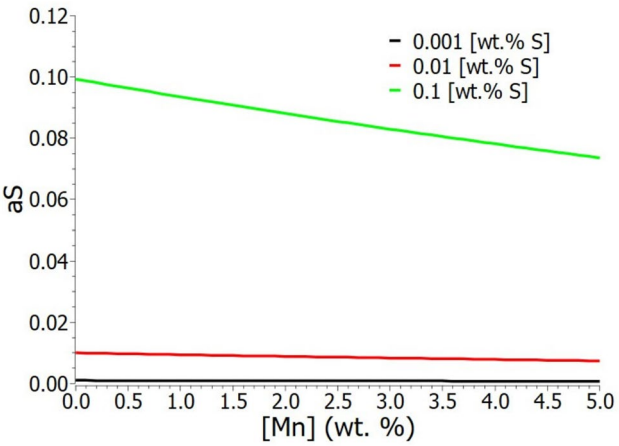

Fig. 8 Influence of manganese addition on sulphur activity

forms more stable CaS [9, 49]. Desulphurisation with magnesium occurs rapidly, in combination with CaO or CaC_2, which also contains CaO, yielding more stable CaS [9, 51, 52]. Figure 7 shows the calculated equilibrium solubility of magnesium and sulphur in the melt at various temperatures. With decreasing temperature of the system, the desulphurisation with magnesium is more effective.

3.3 Manganese Sulphides

Manganese has a high vapour pressure, which means its solubility in the iron melt is also strongly influenced by temperature and the partial pressure above the melt [63]. During the treatment of steel melt in a vacuum, the presence of Mn can lead to the evaporation of the element. Figure 8 shows that the addition of manganese reduces the activity of sulphur in the steel melt, resulting in a lower probability

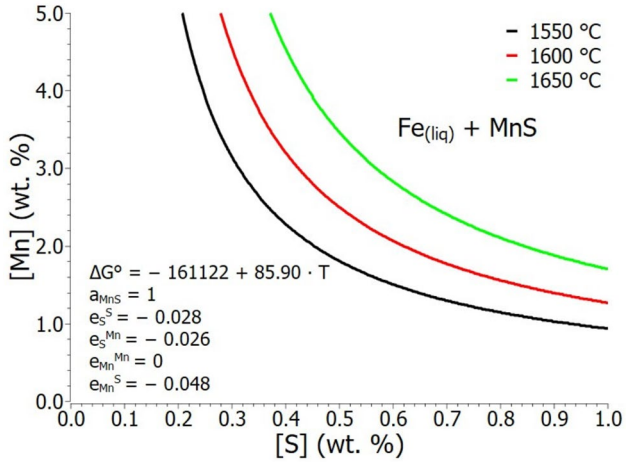

Fig. 9 Equilibrium solubility of Mn and S in liquid iron at different temperatures [1, 2, 28, 29]

of FeS formation. As shown in Fig. 3, manganese forms a sulphide that is more stable than FeS, meaning that with the addition of Mn, the formation of the FeS and the associated issues during hot working, can be effectively reduced.

The solubility of manganese in iron melt is high, leading to the formation of MnS just before or during the solidification of the melt. MnS typically forms in interdendritic spaces during solidification as a result of the segregation of both elements [67–75]. In the literature, there are several segregation models that account for the diffusion of elements and the formation of MnS non-metallic inclusions during the solidification of steels [67–70, 75–77]. The driving force for MnS formation is the supersaturation of the melt with Mn and S, or the high activity of these two elements. As the system temperature decreases, known as undercooling, the equilibrium solubility of Mn and S also decreases, leading to increased supersaturation of the melt. The level of supersaturation influences the shape and size of MnS: at higher supersaturation, fine spherical sulphides form, while lower supersaturation results in dendritic and angular sulphide shapes. In addition to the supersaturation of the steel melt, the morphology of sulphides is influenced by the interfacial tension between the steel melt and non-metallic inclusions. Lower interfacial tension reduces the critical radius size and the energy barrier for nucleation. Alloying elements play an important role as well; they can alter the nucleation mechanism of non-metallic inclusions (e.g., heterogeneous nucleation of MnS on TiN or Al_2O_3) or affect the solidification interval of the steel melt [67, 70, 72, 75, 76].

Figure 9 shows the equilibrium solubility of Mn and S, the solubility of the elements is high, so MnS formation can occur mostly during solidification. During solidification, sulphur and manganese segregation occurs, leading to supersaturation of the melt between formed crystal grains and the nucleation of MnS.

MnS inclusions are solid and exhibit good deformability within the temperature range of hot working, preventing hot shortness in steels. The MnS non-metallic inclusions help break chips during mechanical processing and reduce wear on machining tools [75, 78]. Therefore, sulphur, in combination with manganese, is added to special steel grades to enhance machinability. The presence of MnS non-metallic inclusions in steels accelerates mechanical processing and lowers costs.

4 Conclusions

Understanding the solubility and activity of sulphur is crucial for controlling its concentration, removal from the melt and predicting the sulphide formation. Various thermodynamic methods to determine the solubility of sulphur in liquid iron have been discussed. The solubility of sulphur in liquid steel is difficult to determine due to good solubility in liquid iron. Most of the techniques where we can directly determine sulphur solubility/activity are applicable only in a laboratory environment. Determination via Sievert's law is not possible in industrial practice due to extremely low pressures, in the case of a gas mixture of H_2 and H_2S, such an atmosphere is not in use in the steelmaking practices. The most promising determination is still the chemical analysis of the taken steel samples. The activity of the sulphur can be determined based on the 1 wt% standard state.

The formation of sulphides in the iron melt is strongly linked to the equilibrium solubility of the elements. Mg and Ca have low solubility in iron, and due to their high vapour pressure and low boiling point, sulphides form already in the melt. MnS forms at high concentrations of Mn and S, the formation of the sulphides typically occurs during solidification in interdendritic spaces.

Due to the low solubility of Ca and Mg, direct desulphurisation of steel with these elements is inefficient. In the case of Ca, more promising desulphurisation proceeds with CaO (slag), where the oxide decomposes and forms sulphides. With Mg, sulphide formation is more effective; however, due to the lower stability of the compound, CaO is also added to prevent the re-sulphuration of the melt.

Acknowledgements This research was funded by the Slovenian Research Agency ARRS program P2-0050 (C) and partially by a Milan Lenarčič scholarship.

Author Contributions Conceptualisation: J.B., A.B., literature search and data analysis A.B., original draft preparation: A.B., validation, formal critical analysis: T.B, J.B.

Funding Javna Agencija za Raziskovalno Dejavnost RS,P2-0050 (C),Univerza v Ljubljani,Milan Lenarčič scholarship,Anze Bajzelj

Declarations

Conflicts of interest The authors declare no conflict of interest.

References

1. Turkdogan E T, *London* **656** (1996) 96.
2. S. Seetharaman, A. McLean, R. Guthrie, and S. Sridhar: Treatise on process metallurgy, Industrial Processes, Part A: Volume 3, Elsevier Ltd, Oxford, (2014), 51. ISBN9780333227794
3. Ahindra Ghosh and A. Chatterjee: Ironmaking and Steelmaking: Theory and Practice, PHI Learning Private Limited, New Delhi, (2008), 14. ISBN9788120332898
4. R.H. Tupkary and V.R. Tupkary: Modern Steel Making Handbook, Mercury Learning and Information, Dulles, VA, (2017), 1. ISBN9781683921387
5. Çavuşoğlu B, and Karaca H, *J. Turkish Chem. Soc. B* **1** (2017) 103–114.
6. Yao G, Guo Q, Li Y, Song J, Liu Y, He M, and Qi T, *Powder Technol.* **419** (2023) 118287. https://doi.org/10.1016/j.powtec.2023.118287
7. Zhang Y, Schlangen E, and Çopuroğlu O, *Constr. Build. Mater.* **316** (2022) 125266. https://doi.org/10.1016/j.conbuildmat.2021.125266
8. Rezvani Pour H, Mostafavi A, Shams Pur T, Ebadi Pour G, and Haji Zadeh Omran A, *Physicochem. Prob. Min. Proc.* **52** (2016) 845–854.
9. Schrama F N H, Beunder E M, Van den Berg B, Yang Y, and Boom R, *Ironmak. Steelmak.* **44** (2017) 333–343. https://doi.org/10.1080/03019233.2017.1303914
10. Moosavi-Khoonsari E, Van Ende M A, and Jung I H, *Metall. Mater. Trans. B* **53** (2022) 981–998. https://doi.org/10.1007/s11663-022-02437-1
11. Turkdogan E T, and Martonik L J, *Trans. ISIJ Int.* **23** (12), (1983) 1038–1044. https://doi.org/10.2355/isijinternational1966.23.1038
12. Guo Z, Fu Z, and Wang S, *Fuel Process. Technol.* **88** (2007) 935–941. https://doi.org/10.1016/j.fuproc.2007.05.003
13. Chou C L, *Int. J. Coal Geol.* **100** (2012) 1–13. https://doi.org/10.1016/j.coal.2012.05.009
14. Waldner P, and Pelton A D, *J. Phase Equilibria Diffus.* **26** (2005) 23–38. https://doi.org/10.1361/15477030522455
15. Hillert M, and Staffansson L I, *Metall. Trans. B* **6** (1975) 37–41. https://doi.org/10.1007/BF02825676
16. Sharma R C, and Chang Y A, *Metall. Trans. B* **10** (1979) 103–108. https://doi.org/10.1007/BF02653979
17. Guillermet A F, Hillert M, Jansson B, and Sundman B, *Metall. Trans. B* **12** (1981) 745–754. https://doi.org/10.1007/BF02654144
18. Kongoli F, Dessureault Y, and Pelton A D, *Metall. Mater. Trans. B* **29** (1998) 591–601. https://doi.org/10.1007/s11663-998-0094-y
19. Kongoli F, and Felton A D, *Metall. Mater. Trans. B* **30** (1999) 443–450. https://doi.org/10.1007/s11663-999-0077-7
20. Chuang Y Y, Hsieh K C, and Chang Y A, *Metall. Trans. B* **16** (1985) 277–285. https://doi.org/10.1007/BF02679718
21. O. Kubaschewski: IRON - Binary Phase Diagrams, Springer, Aachen, (1982), 125. ISBN9783662080269
22. Fincham C J B, and Richardson F D, *Proc. R. Soc. London. Ser. A. Math. Phys. Sci.* **223** (1954) 40–62. https://doi.org/10.1098/rspa.1954.0099
23. Kang Y B, *Metall. Mater. Trans. B* **52** (2021) 2859–2882. https://doi.org/10.1007/s11663-021-02224-4
24. Waldner P, *Int. J. Mater. Res.* **106** (2015) 352–360. https://doi.org/10.3139/146.111185
25. Burja J, Koležnik M, Župerl Š, and Klančnik G, *Mater. Tehnol.* **53** (6), (2019) 919–928. https://doi.org/10.17222/mit.2019.247
26. Sherman C W, Elvander H I, and Chipman J, *JOM* **188** (1950) 334–340. https://doi.org/10.1007/bf03399008
27. Hu G, Dam-Johansen K, Wedel S, and Hansen J P, *Prog. Energy Combust. Sci.* **32** (2006) 295–314. https://doi.org/10.1016/j.pecs.2005.11.004
28. I. Barin: Thermochemical Data of Pure Substances, Third ed., VCH Verlagsgesellschaft mbH, Weinheim, (1995), 1. ISBN3527287450
29. Sigworth G K, and Elliott J F, *Met. Sci.* **8** (1974) 298–310. https://doi.org/10.1179/msc.1974.8.1.298
30. The Japan Society for the Promotion of Science The 19th Committee on Steelmaking: Steelmaking Data Sourcebook, Gordon and Breach Science Publisher, New York, (1988), 1. ISBN2881241530
31. Chang Y A, Fitzner K, and Zhang M X, *Prog. Mater. Sci.* **32** (1988) 97–259. https://doi.org/10.1016/0079-6425(88)90001-1
32. Ikada S, Hayashi S, and Uno T, *Tetsu-To-Hagane* **61** (1975), (1975) 2321–2327. https://doi.org/10.2355/tetsutohagane1955.61.10_2321. ((**in Japanese**)).
33. Ishii F, and Fuwa T, *Tetsu-To-Hagane* **67** (1981) 736–745. https://doi.org/10.2355/tetsutohagane1955.67.6_736. ((**in Japanese**)).
34. Ishii F, and Fuwa T, *Tetsu-To-Hagane* **67** (1981) 746–754. https://doi.org/10.2355/tetsutohagane1955.67.6_746. ((**in Japanese**)).
35. Shohoji N, *Trans. ISIJ Int. Japan* **26** (1986) 547–550. https://doi.org/10.2355/isijinternational1966.26.547
36. Hong Y R, Jin C J, Li L S, and Sun J L, *Sensors Actuators B Chem.* **87** (2002) 13–17. https://doi.org/10.1016/S0925-4005(02)00174-0
37. Wen T, Yu J, Yuan L, Jin E, Liu T, Tian C, and Zhou Y, *Ceram. Int.* **46** (2020) 4256–4264. https://doi.org/10.1016/j.ceramint.2019.10.146
38. Wen T, Yu J, Jin E, Liu T, Hou X, and Sun Q, *Sensors Actuators B Chem.* **279** (2019) 177–182. https://doi.org/10.1016/j.snb.2018.09.124
39. C. Wagner: Thermodynamics of Alloys, Addison-Wesley Press, Massachusetts, (1952), 1. ISBN9780201084306
40. Lupis C H P, and Elliott J F, *Acta Metall.* **14** (1966) 529–538. https://doi.org/10.1016/0001-6160(66)90320-8
41. S. Seetharaman: Treatise on Process Metallurgy, Volume 1: Process Fundamentals, Elsevier, Oxford, (2013), 629. ISBN9780080969862
42. Liu Y, Zhang L, Zhang Y, Duan H, Ren Y, and Yang W, *Metall. Mater. Trans. B* **49** (2018) 610–626. https://doi.org/10.1007/s11663-018-1179-x
43. Wang H Y, Hou Y, Zhang G H, and Chou K C, *ISIJ Int.* **60** (2020) 636–639. https://doi.org/10.2355/isijinternational.ISIJINT-2019-453

44. Hayashi S, and Uno T, *Tetsu To Hagane* **68** (1982) 1728–1736. https://doi.org/10.2355/tetsutohagane1955.68.13_1728. ((**in Japanese**)).
45. Taguchi K, Ono-Nakazato H, Nakai D, Usui T, and Marukawa K, *ISIJ Int.* **43** (2003) 1705–1709. https://doi.org/10.2355/isijinternational.43.1705
46. Han Q, Zhang X, Chen D, and Wang P, *Metall. Trans. B* **19** (1988) 617–622. https://doi.org/10.1007/BF02659153
47. Speer M C, and Parlee A D, *AFS Cast Met Res J.* **20** (1972) 122–128.
48. Debi Z, and Qiyong H, *Chin. J. Eng.* **17** (1995) 576–579. https://doi.org/10.13374/j.issn1001-053x.1995.06.017. ((**in Chinese**)).
49. Yang J, Kuwabara M, Teshigawara T, and Sano M, *ISIJ Int.* **45** (2005) 1607–1615. https://doi.org/10.2355/isijinternational.45.1607
50. Matsushita N, Awaya K, Saito K, and Hasegawa M, *ISIJ Int.* **61** (2021) 2929–2936. https://doi.org/10.2355/isijinternational.ISIJINT-2021-247
51. Magnelöv M, Eriksson J, Drugge J, Björkvall J, and Björkman B, *Ironmak. Steelmak.* **40** (2013) 436–442. https://doi.org/10.1179/1743281212Y.0000000067
52. Magnelöv M, Carlsson-Dahlberg A, Gustavsson L, Björkvall J, and Björkman B, *Ironmak. Steelmak.* **42** (2015) 525–532. https://doi.org/10.1179/1743281214Y.0000000257
53. Han Q, Zhou D, and Xiang C, *Steel Res. Int.* **68** (1997) 9–14. https://doi.org/10.1002/srin.199701770
54. Lu Y, and Miki T, *ISIJ Int.* **61** (2021) 2360–2369. https://doi.org/10.2355/isijinternational.ISIJINT-2021-088
55. Choudhary S K, and Ghosh A, *ISIJ Int.* **48** (2008) 1552–1559. https://doi.org/10.2355/isijinternational.48.1552
56. Zhao B, Wu W, Yang F, Zeng J, Liang Z, and He J, *Metall. Mater. Trans. B* **55** (2024) 1244–1260. https://doi.org/10.1007/s11663-024-03005-5
57. Gong W, Jiang Z, Zhang L, Chen C, and Dong Y, *Mater. Sci. Eng. A* **791** (2020) 139410. https://doi.org/10.1016/j.msea.2020.139410
58. Suito H, and Inoue R, *ISIJ Int.* **36** (1996) 528–536. https://doi.org/10.2355/isijinternational.36.528
59. Fujiwara H, Tano M, Yamamoto K, and Ichise E, *ISIJ Int.* **35** (1995) 1063–1071. https://doi.org/10.2355/isijinternational.35.1063
60. Trojan P K, and Flinn R A, *SAE Automotive Engineering Congress* **73** (1965) 265–272. https://doi.org/10.4271/640802
61. Yang J, Ozaki S, Kakimoto R, Okumura K, Kuwabara M, and Sano M, *ISIJ Int.* **41** (2001) 945–954. https://doi.org/10.2355/isijinternational.41.945
62. Gran J, and Sichen D, *Metall. Mater. Trans. B* **42** (2011) 921–924. https://doi.org/10.1007/s11663-011-9557-7
63. Zhang Z, Wang Z, Miao R, Zhu Q, Chen D, Zhang X, Zhou L, Li Z, and Yan S, *Vacuum* **107** (2014) 77–82. https://doi.org/10.1016/j.vacuum.2014.04.007
64. Zhang T, Liu C, Mu H, Li Y, and Jiang M, *Ironmak. Steelmak.* **45** (2018) 447–456. https://doi.org/10.1080/03019233.2017.1284420
65. Su J, Dou Z, Zhang T, and Liu Y, *J. Iron Steel Res. Int.* **27** (2020) 1391–1399. https://doi.org/10.1007/s42243-020-00507-9
66. Irons G A, and Guthrie R I L, *Metall. Trans. B* **12** (1981) 755–767. https://doi.org/10.1007/BF02654145
67. Oikawa K, Ohtani H, Ishida K, and Nishizawa T, *ISIJ Int.* **35** (1995) 402–408. https://doi.org/10.2355/isijinternational.35.402
68. Tanaka Y, Pahlevani F, Moon S C, Dippenaar R, and Sahajwalla V, *Sci. Rep.* **9** (2019) 10096. https://doi.org/10.1038/s41598-019-46450-y
69. You D, Michelic S K, Presoly P, Liu J, and Bernhard C, *Metals* **7** (2017) 460. https://doi.org/10.3390/met7110460
70. You D, Michelic S K, Wieser G, and Bernhard C, *J. Mater. Sci.* **52** (2017) 1797–1812. https://doi.org/10.1007/s10853-016-0470-y
71. You D, Bernhard C, Bernhard M, and Michelic S K, *J. Mater. Res. Technol.* **28** (2024) 4110–4115. https://doi.org/10.1016/j.jmrt.2024.01.029
72. Diederichs R, and Bleck W, *Steel Res. Int.* **77** (2006) 202–209. https://doi.org/10.1002/srin.200606375
73. Diederichs R, Bülte R, Pariser G, and Bleck W, *Steel Res. Int.* **77** (2006) 256–264. https://doi.org/10.1002/srin.200606383
74. Valdez M E, Wang Y, and Sridhar S, *Steel Res. Int.* **75** (2004) 247. https://doi.org/10.1002/srin.200405952
75. Chu J, Zhang L, Yang J, Bao Y, Ali N, and Zhang C, *Mater. Charact.* **194** (2022) 112367. https://doi.org/10.1016/j.matchar.2022.112367
76. Zhang H, Feng G, Liu X, Wang B, and Liu X, *Metals* **10** (2020) 570. https://doi.org/10.3390/met10050570
77. Shu Q, Visuri V V, Alatarvas T, and Fabritius T, *Metall. Mater. Trans. B* **51** (2020) 2905–2916. https://doi.org/10.1007/s11663-020-01955-0
78. Shin J H, and Park J H, *Metall. Mater. Trans. B* **49** (2018) 311–324. https://doi.org/10.1007/s11663-017-1152-0